J. Mol. Biol. (1994) **239**, 689–697

Electron Cryomicroscopy of *Bacillus stearothermophilus* 50 S Ribosomal Subunits Crystallized on Phospholipid Monolayers

Agustin J. Avila-Sakar[1], Ting-Lu Guan[2]†, Talmon Arad[3], Michael F. Schmid[2] Tim W. Loke[2], Ada Yonath[3,4], Jutta Piefke[5], François Franceschi[5] and Wah Chiu[1,2]‡

[1]*Department of Molecular Physiology and Biophysics and The Keck Center for Computational Biology, Baylor College of Medicine, One Baylor Plaza, Houston, TX 77030, U.S.A.*

[2]*Verna and Marrs McLean Department of Biochemistry and The Keck Center for Computational Biology, Baylor College of Medicine, One Baylor Plaza, Houston, TX 77030, U.S.A.*

[3]*Department of Structural Biology, Weizmann Institute of Science, Rehovot, Israel*

[4]*Max-Planck-Laboratory for Ribosomal Structure, Hamburg, Germany*

[5]*Max-Planck-Institute for Molecular Genetics, D-1000 Berlin 33, Germany*

50 S ribosomal subunits from *Bacillus stearothermophilus* have been crystallized as 2-dimensional periodic arrays on phospholipid monolayer films at the water-air interface. These crystals were preserved in vitreous ice and imaged with 100 keV electrons under low dose and low temperature conditions. The unit cell parameters of the crystals are $a=371{\cdot}3(\pm3{\cdot}8)$ Å, $b=152{\cdot}3(\pm1{\cdot}6)$ Å, $\gamma=96{\cdot}3(\pm1{\cdot}0)°$. Some of the image arrays of these crystals have twofold rotational symmetry with a phase residual of less than 25°. The mean figure of merit of the merged structure factors from these image arrays out to 20 Å resolution is higher than 0·87. The 2-dimensional projection map shows a level of detail not seen in previous structural studies of the 50 S ribosome subunit. Some of these features may be related to the current 3-dimensional model of the subunit. This analysis illustrates the potential of using the electron crystallographic approach for determining the 3-dimensional structure of the 50 S ribosomal subunit crystallized on a monolayer surface. In addition, the structural information retrieved by electron crystallography might be useful for phasing X-ray data towards an atomic resolution model of the ribosome.

Keywords: 50 S ribosomal subunit; 2-dimensional crystals; electron crystallography

1. Introduction

The ribosome is a subcellular organelle, which plays a key role in protein synthesis. This large and complex structure carries out a uniquely intricate function that matches the complexity of the translation of the genetic code. A typical bacterial ribosome contains 56 to 73 proteins and 3 rRNA molecules (for a review, see Hill *et al.*, 1990). Understanding their spatial organization is essential to unravel the mechanism of the biological processes involved in the translation of the genetic code into proteins.

In the past two decades, structural studies of the whole ribosome and of its two subunits from various organisms have been carried out by a variety of methods (for reviews see Hardesty & Kramer, 1986; Hill *et al.*, 1990), including X-ray crystallography (Berkovitch-Yellin *et al.*, 1992), neutron scattering (Capel *et al.*, 1988; May *et al.*, 1992), and three-dimensional reconstruction from electron microscopic images of dispersed single particles (Frank *et al.*, 1990, 1991), or of two-dimensional arrays (Milligan & Unwin, 1986; Yonath *et al.*, 1987; Arad *et al.*, 1987; Berkovitch-Yellin *et al.*, 1990). As a result, our knowledge base has increased steadily, particularly about the overall shape of the ribosome. Furthermore, the locations of several functional domains, involved in binding tRNA and mRNA as well as the path of the nascent peptides, have been proposed (for a review, see Yonath & Berkovitch-Yellin, 1993).

† Present address: Department of Cell & Molecular Biology, The Scripps Research Institute, 10666 N. Torrey Pines Road, La Jolla, CA 92037, U.S.A.

‡ Author to whom all correspondence should be addressed.

0022-2836/94/250689-09 $08.00/0

The successful growth of 3-dimensional crystals of 50 S subunits from *Haloarcula marismortui*, diffracting to 3 Å resolution (von Böhlen *et al.*, 1991), presents reasonable prospects of visualizing the atomic structure of this ribosomal subunit. However, the ribosomal particles are large, and they lack the non-crystallographic symmetry which has facilitated structure determination in crystals of large specimens such as icosahedral virus particles. The phasing of diffraction intensities by the conventional approach of multiple isomorphous replacement technique should be rather complicated. Therefore, a number of alternative phasing approaches are being pursued. These include genetic engineering to produce ribosome mutants capable of binding multi heavy atom clusters and exploring the use of models obtained by other structural techniques for the initial steps in phasing (Berkovitch-Yellin *et al.*, 1992).

The growth of two-dimensional arrays of prokaryotic ribosomal particles has been reported earlier (Clark *et al.*, 1982; Arad *et al.*, 1984, 1987; Yonath *et al.*, 1987). Among the various species tried, ribosomes from thermophilic bacteria have been more successful because of their greater stability, as opposed to the unstable *Escherichia coli* particles, on which most of the biochemical studies have been done (for a review, see Berkovitch-Yellin, *et al.*, 1992). However, reconstructions have yielded rather low resolution models, namely 30 Å to 50 Å. This relatively poor order might be due to the heterogeneity of ribosome populations (Tumminia *et al.*, 1991) or to the inherent flexibility of the ribosomal particles, as well as to the quality of the crystalline arrays induced by crystallization conditions different from the ribosomes' natural chemical environment. All these studies were carried out using negative stain preparations. Therefore the measured property was stain exclusion. In addition, these studies were performed without using optimal procedures to minimize radiation damage.

In the investigation reported here, we attempted to obtain crystalline samples of higher quality, suitable for high resolution electron crystallographic analysis, by inducing crystallization of 50 S ribosomal subunits from *Bacillus stearothermophilus* on lipid monolayer films. This crystallization procedure has proven to be suitable for a number of soluble proteins (see reviews, see Kornberg & Darst, 1991; Jap *et al.*, 1992). In the case of streptavidin, crystalline arrays yielded electron diffraction beyond 3 Å resolution (Kubalek *et al.*, 1991; Chiu, 1993). Since ribosomes are composed of components with different densities, namely proteins and RNA, we may be able to use a 3-dimensional map reconstructed from data collected from ice-embedded specimens to develop powerful models with a dual envelope for phase extension algorithms. This is not possible for a negative stain structure where stain exclusion arises from both RNA and protein about equally. Moreover, the studies performed on ordered arrays (Milligan & Unwin, 1986) or single particles (Frank *et al.*, 1991) so far in vitreous ice were at a resolution insufficient to provide an accurate envelope for RNA and for protein separately.

2. Materials and Methods

(a) *Preparation and crystallization of the 50 S ribosomal subunits*

The preparation and the storage of 50 S ribosomal subunits have been previously described (Yonath *et al.*, 1987). Crystallization was carried out in a Teflon trough (4 mm diameter, 1 mm depth) with a total volume of ~20 μl. The composition of the crystallization buffer was 300 mM to 600 mM NaCl, 20 mM $CaCl_2$, 20 mM to 90 mM $MgCl_2$ (*in* H-I buffer, Yonath *et al.* (1987), pH 6·0 to 6·5). An amount (20 μl) of a 0·3 to 0·5 mg/ml suspension of 50 S ribosomal subunits was deposited in the trough for the crystallization. These conditions are similar to those used for long-term storage of ribosomes, and are thus not likely to promote dissociation of ribosomes, at least in the absence of lipid. Purified dioleoyl-phosphatidylserine (DOPS) and dioleoylphosphatidylcholine (DOPC) were obtained from Avanti (Alabama, U.S.A.). A mixture of DOPS and DOPC at a ratio of 1 : 4 or 1 : 5 and a total concentration of 0·5 to 1·0 mg/ml in either chloroform or hexane was deposited on top of the crystallization solution to form a monolayer film at the water-air interface. The trough was kept in a moist chamber at 4 to 7 °C for 1 to 3 weeks.

(b) *Electron cryomicroscopy*

Carbon coated holey grids with holes of 1 to 2 μm in diameter were placed gently on top of the lipid-protein solution. After 1 to 3 minutes the grids were picked up with care and the excess liquid was blotted for either negative stain (0·5% uranyl acetate) or for rapid freezing in liquid ethane (Adrian *et al.*, 1984; Jeng *et al.*, 1988; also see Chiu, 1986; Dubochet *et al.*, 1988; for a more extensive review on microscopy of vitrified specimens). Negative stain microscopy was used just for monitoring crystal growth. A Gatan cryoholder was used to keep the frozen, hydrated specimens at a temperature of −150 °C. Electron micrographs were taken with 100 keV electrons at a nominal magnification of 30,000×, with less than 8 electrons/Å^2 using conventional low dose procedures similar to those described previously (Jeng & Chiu, 1983) in a JEOL1200 electron microscope. Kodak SO163 films were used for recording the images and were developed in D19 at 20 °C. The electron micrographs were evaluated in an optical diffractometer for their resolution and image quality.

(c) *Computer image processing*

Three electron micrographs of the crystalline arrays of the 50 S ribosomal subunits, embedded in vitreous ice, were chosen for computer processing. They were digitized using a Perkin-Elmer microdensitometer 1010M, at a sampling distance equivalent to 3·3 Å in the object. Because obvious crystal defects were detected in different regions of the large crystalline patches, we restricted computer processing to 1024^2 pixel array, which corresponds roughly to 200 unit cells. Each digitized micrograph contained about 45 to 50 such arrays. Each of the arrays was visualized in real and Fourier space to assess its apparent quality. Seventy-six arrays from the three micrographs were selected for further analysis using the UNIX based software system SPECTRA, which is an

interactive graphic interface for indexing reflections, refining reciprocal lattice parameters, generating a filtered image, computing a correlation map with a reference image, searching for correlation peak positions, unbending the original image and computing the final structure factors (Schmid *et al.*, 1993*a*). All computations were done on a Silicon Graphics power series 320 processor. Graphic displays were done on a NCD color X-terminal or an Indigo R4000 workstation.

In order to determine the contrast transfer function we summed the amplitudes of Fourier transforms of all digitized arrays of each single micrograph (Zhou, 1993). When the contrast transfer function rings were visible in the summed spectrum, appropriate phase reversals were done and the amplitude correction was made using a Wiener filter (Schmid *et al.*, 1991).

At the beginning of the analysis of the images, we searched for possible variations in the unit cell motif in individual or different micrographs. The level of similarity between the various motifs was evaluated initially by phase coherence of the reflections in the Fourier transforms among different arrays. We employed a relatively stringent criterion to assign the similarity among different arrays into groups. It was required that the phase residual for reflections with $IQ \leq 4$ from different arrays within a group be less than 25°. IQ is an index describing the signal/noise ratio of individual reflections, with $IQ = 1$ equivalent to a signal/noise ratio better than 8 and $IQ = 8$ equivalent to a signal which is equal to or less than the local background. $IQ = 4$ corresponds approximately to a signal which, after background subtraction, is twice as strong as the local background (Henderson *et al.*, 1986). The reflections in groups which fulfilled that criterion were added vectorially to yield a composite structure factor. The mean figures of merit of the merged structure factors were calculated in different resolution zones using phase probability estimates (Henderson *et al.*, 1986) in order to quantify the reliability and reproducibility of the observed reflections. To show the diffraction strength of the data, the logarithm of the merged amplitudes of reflections *versus* the square of the spatial frequency was plotted. The merged structure factors in different merging groups were further characterized for the presence of twofold rotational symmetry about an axis normal to the projection plane using various resolution limits (Robinson *et al.*, 1988). Projection density maps were computed from the group that had a twofold rotational symmetry phase residual less than 25°.

3. Results and Discussion

The exact mechanisms of the formation of highly ordered 2-dimensional crystalline arrays of biological macromolecules on phospholipid films are still not well understood. In some cases, it may require a special ligand to which the protein binds with high affinity, as exemplified by the formation of monolayers of tetanus toxin and botulism toxin using ganglioside as ligand (Robinson *et al.*, 1988; Schmid *et al.*, 1993*c*) and of streptavidin on biotinylated lipid layers (Darst *et al.*, 1991*a*). In other cases, the macromolecule exploits surface charges of the lipid film which may generate a favorable chemical environment for lattice interactions, as in the cases of RNA polymerase (Darst *et al.*, 1991*b*) and of α-actinin (Taylor & Taylor, 1993). The formation of the 50 S ribosomal subunit crystalline arrays is thought to have occurred by the second mechanism. Figure 1 shows portions of three

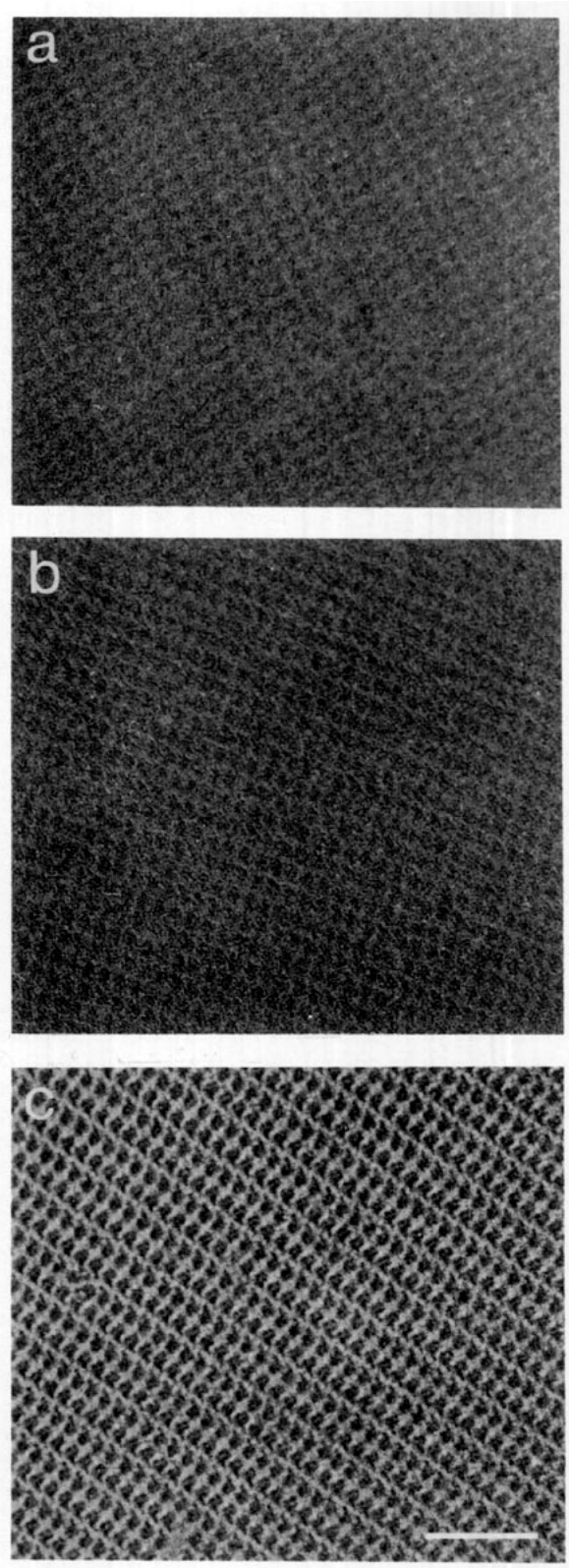

Figure 1. 100 kV electron images of ice-embedded crystalline arrays of 50 S ribosomal subunits, taken at different defocus values from three different arrays. Ribosomal subunits are dark. Scale bar represents 1000 Å.

separate micrographs of crystalline arrays of 50 S ribosomal subunits embedded in vitreous ice taken at different defocus conditions. A visual inspection of the micrographs suggests that these arrays are likely to be composed of monolayers of 50 S ribosomal particles. Some of these crystals extend over an area of several μm^2. Nevertheless, they have obvious crystal defects, which make them impractical to be studied by high resolution electron diffraction analysis. However, we can extract small areas which are reasonably well-ordered and suitable for analysis by Fourier averaging. The low resolution features of these three images appear dissimilar probably because of the difference in defocus and ice thicknesses. In all cases, they exhibit visible contrast, particularly in the highly defocused images (Figure 1c).

The average unit cell parameters were estimated to be $a=371{\cdot}3(\pm 3{\cdot}8)$ Å, $b=152{\cdot}3(\pm 1{\cdot}6)$ Å, $\gamma=96{\cdot}3(\pm 1{\cdot}0)°$. These lattice parameters were measured from the reciprocal lattice in the Fourier transforms of 76 image arrays of 1024×1024. The calibration of these values were derived from the magnification of the image read out from the microscope panel and the scanning spot size of the microdensitometer. The unit cell dimensions and the apparent twofold rotational symmetry of these monolayers are very similar to those of the previously obtained two-dimensional arrays of the same particles, though they were grown under completely different conditions (Yonath *et al.*, 1987). Since tilt series of the latter were used for three-dimensional image reconstruction, their thickness ($\sim$190 to 220 Å) was determined directly from the three-dimensional map. Based on this information, we estimate the thickness of the current monolayers to be of a similar magnitude.

The contrast transfer function rings were not apparent in optical diffractograms of an image area of 1 μm (in terms of the specimen) in diameter. To enhance the visibility of the contrast transfer function rings, we summed the amplitudes of computed Fourier transforms of individual image arrays from the same micrograph. We found that not all images gave rise to the contrast transfer (CTF) rings. In the case of images taken at large defocus values (for example, 6·9 μm), the CTF rings became readily visible after summation, and the phases were corrected accordingly. However, in images taken closer to focus, such rings were not discernible in the summed amplitude files. Therefore, our approach was to merge first the structure factors coming from image arrays where the defocus could be determined, and then to merge in the phases from other arrays in resolution zones, up to the point where the phase residual increased above 25°. The data used in the map shown below are coherent by this criterion up to 20 Å.

In the image processing procedure, we could in principle process a large image array of 6000×6000, as commonly practiced in images of highly ordered crystals (Henderson *et al.*, 1986, 1990). At the early stage of analysis, we used that approach and have found a large phase residual in the merging of the structure factors of the images. Therefore, we divided the images into many small arrays of 1024×1024. In each of them, we applied the unbending procedure. We found that unbending of the raw image arrays generally helped to retrieve more reflections with high signal/noise values, as previously shown (Henderson *et al.*, 1986). The unbent image arrays could be classified into several groups according to the phase similarity among their structure factors. We used the merging phase residual under the assumption of $p1$ symmetry as a criterion to classify arrays into groups. Each group had an overall merging phase residual of less than 25°. We then evaluated the merged structure factors of each group for possible rotational symmetry. The phase residual for a twofold rotation axis normal to the plane was found to range from 20° to 37° among the groups up to 20 Å resolution. In other words, some regions of the image have motifs related by excellent twofold rotational symmetry perpendicular to the projection plane in a unit cell, while others have a less strict symmetry relationship. The fact that different parts of a single extended crystalline array do not share exactly the same symmetry could be due to different motifs of the ribosomal subunits in the unit cells. The origin of this structural variation is unclear. It might be a reflection of the heterogeneity inherent in ribosomal populations (Tumminia *et al.*, 1991). It is also possible that the flexible ribosomal particles assume different conformational states while crystallizing on the phospholipid monolayer or are captured under slightly different conformations at the moment of freezing. Alternatively, the subunits could have a rather stable internal conformation but may assume some variability on the monolayer film. A fourth possibility is bending of the crystals so that some regions do not lie perpendicular to the beam, lowering the twofold symmetry. Furthermore, images from different areas of the crystalline array exhibit different extent of defocus, astigmatism or drift which can be caused by charging and beam-induced movements. In any case, these deviations reduce the long range order of the crystal. This explains why we could not use a large image array for detailed analysis.

We combined the structure factors of image arrays with the best twofold rotational symmetry. The reliability of these merged reflections is displayed in Figure 2 in terms of their figures of merit as previously defined (Henderson *et al.*, 1986). 90% of the expected reflections up to 20 Å, and 44% of the data between 20 and 15 Å exhibit a figure of merit $\geq 0{\cdot}87$. A plot of the logarithm of the diffraction amplitudes *versus* the square of the spatial frequency, similar to the Wilson plot of X-ray crystallography, confirms that some of our image data extend well beyond 20 Å (Figure 3). The strength of the structure factors decays to the level of noise at around 15 Å. The fall-off of the diffraction amplitudes might be caused by instrumental factors such as the spatial coherence effect, but

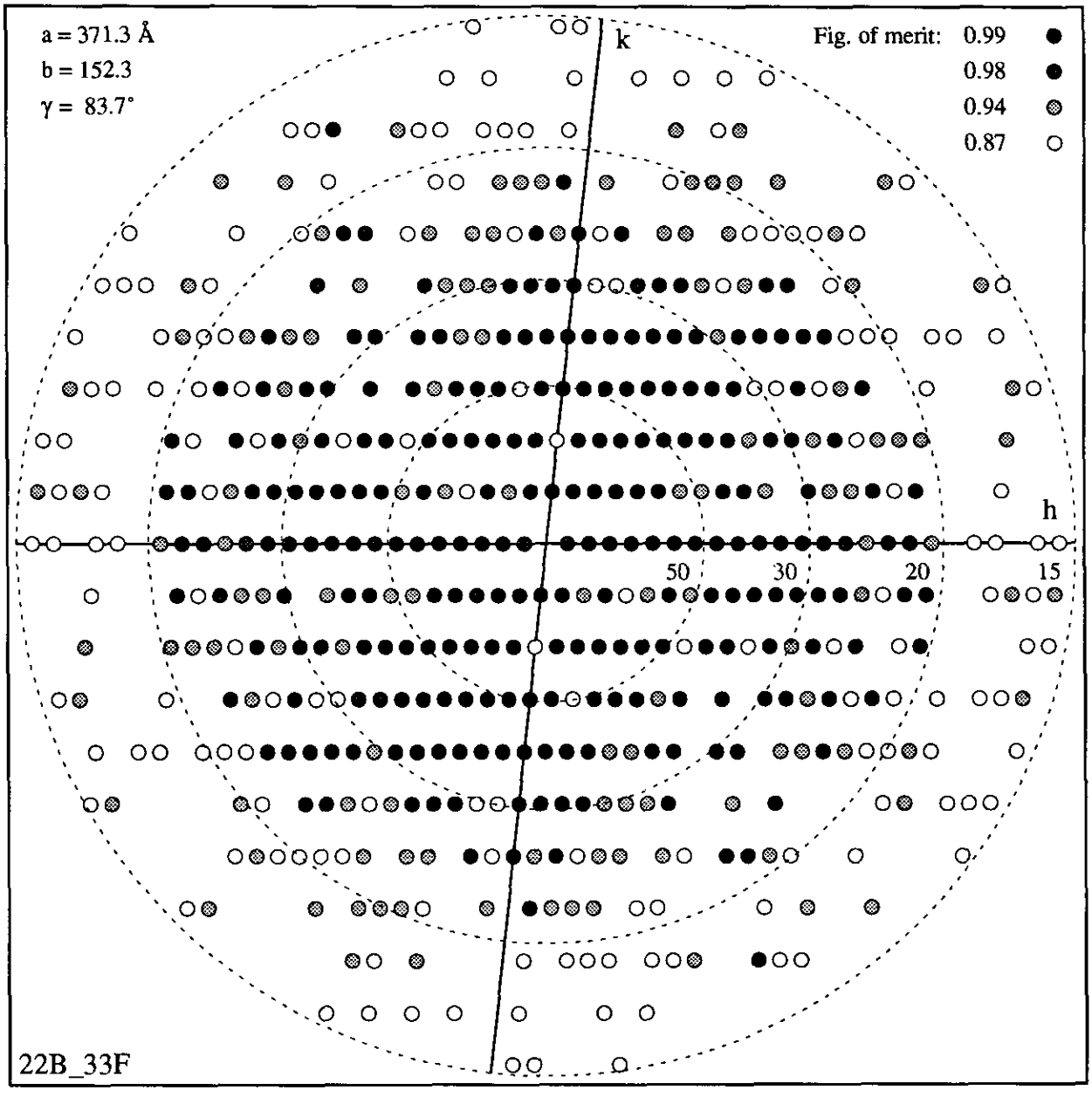

Figure 2. Diagramatic representation of the merged structure factors from 10 image arrays with a total of 2070 unit cells, in terms of mean figure of merit. 90% of the expected reflections up to 20 Å resolution have a mean figure of merit ≥0·87. Between 20 and 15 Å, only 44% of the data have such a mean figure of merit. Such a reduction could arise from imaging conditions or from weaker structure factors. $p2$ symmetry phase residual for the structure factors up to 20 Å resolution is 24°.

might also reflect a weakening of the structure factors themselves (Henderson, 1992).

A projection density map, constructed with the merged data exhibiting twofold symmetry up to 20 Å is shown in Figure 4. We have used data up to 20 Å because we are confident that there is no phase reversal from the contrast transfer function up to that resolution (see above). Even though no symmetry enforcement was applied, a twofold rotation axis normal to the plane of the monolayer relating the two ribosomal subunits in each unit cell can be visualized. Interestingly, the other types of two-dimensional arrays obtained so far from ribosomal particles from *B. stearothermophilus* also showed apparent twofold rotational symmetry, regardless of the method and conditions used for crystal growth. These include not only two forms of arrays obtained from 50 S subunits (Arad *et al.*, 1984; Yonath *et al.*, 1987) but also from entire 70 S ribosomes (Arad *et al.*, 1987).

As seen in Figure 4, the projection density map reveals significant detail which had not been observed in previous structural studies of the ribosomal 50 S subunits. For a clearer representation of the mass density, we replotted one of the ribosomal subunits in the unit cell in color (Figure 5). This particular projection view does not seem to correspond to a characteristic, conventional view of the

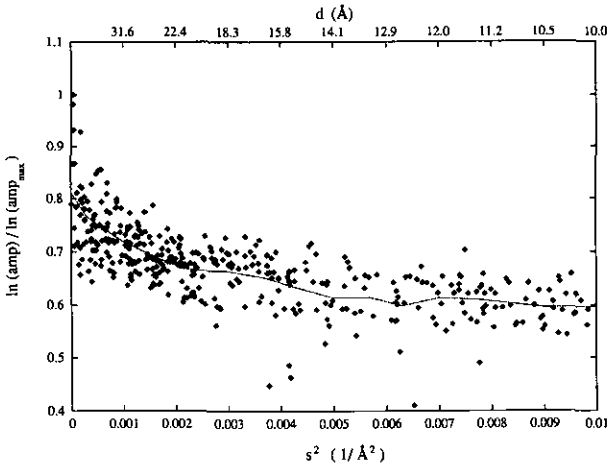

Figure 3. Logarithm of the merged amplitudes as a function of the square of the spatial frequency. The data shown are from the same 10 image arrays as in Figure 2. They have mean figures of merit $\geq 0{\cdot}87$ and apparent $p2$ symmetry. The strength of the structure factors decays to the level of noise at about 15 Å, suggesting that the resolution of our present data is about 15 Å.

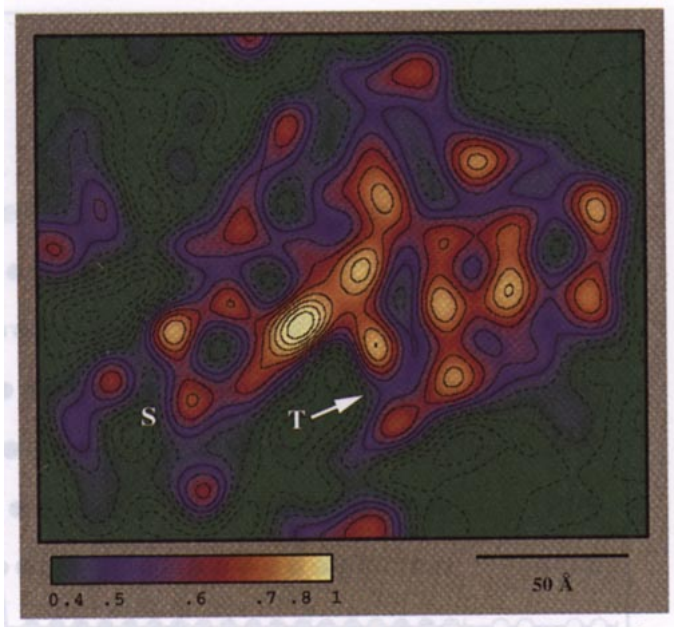

Figure 5. A color display of a single 50 S ribosomal subunit highlighting the dense regions. Some of those dense regions may have a high content of rRNA. Yellow color indicates high density and green color indicates low density. Relative density values can be read from the color bar. Contours traced with continous lines have relative densities above 0·5 on a 0·0 to 1·0 scale. This projection does not appear to correspond to any characteristic view of the 50 S ribosomal subunit. The protrusion (labeled S) may include the stalk, identified by comparison to a low-resolution reconstruction using a truncated data set, shown in Figure 6. This allows us to make a rough estimation of the orientation of the particle, with the translational domain towards the lower part of the Figure. The arrow points to an internal low density region, which may be the entrance of the tunnel (T) which is thought to be the path of the nascent polypeptides (Yonath *et al.*, 1987; Yonath & Wittmann, 1989).

50 S subunit, as described from negatively stained particles on carbon films (see, for example, Verschoor *et al.*, 1985; Harauz *et al.*, 1987), but may be similar to that reconstructed from the two-dimensional arrays (Yonath *et al.*, 1987). To establish a correspondence between the projected density and the overall shape of the 50 S ribosomal particle, Figure 6 displays the same projected structure, but with a sharp cut-off of reflections at 50 Å resolution. This resolution truncation yields a map similar to that with a Gaussian fall-off applied to reflections beyond 30 Å (data not shown). It contains a feature which may correspond to that known as "the stalk", (labeled S in Figure 5), in a configuration similar to that seen in the reconstructed images from the two-dimensional arrays and from the ice-embedded single particles (Radermacher *et al.*, 1992). Alternatively, it could represent a projection of the entire top of the "crown", including the stalk

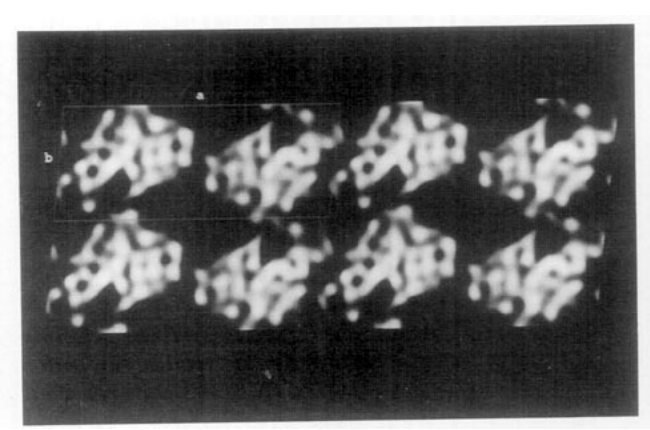

Figure 4. Projection density map of the 50 S ribosome crystal with merged structure factors out to 20 Å resolution. The ribosomal mass density is shown in white and the embedding ice in black. There are two ribosomal subunits per unit cell related by a twofold rotation axis normal to the plane. No symmetry enforcement was made. A single unit cell is outlined in the Figure. Unit cell dimension are $a = 371$ Å, $b = 152$ Å, $\gamma = 96°$.

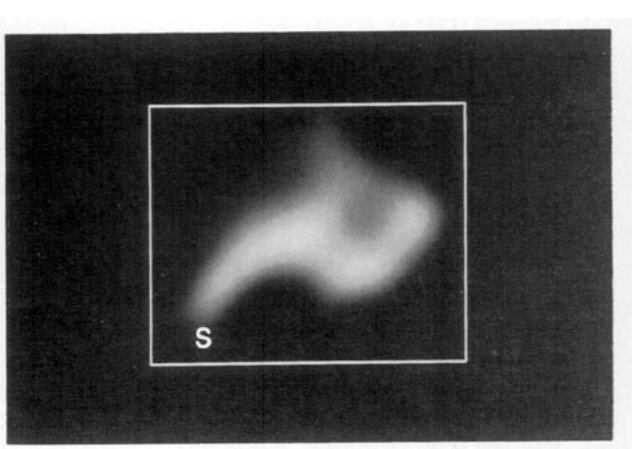

Figure 6. 2-dimensional projection map of one 50 S ribosomal subunit at a resolution of 50 Å. The protrusion (S) can be more readily recognizable from this map.

and other protrusions, in an orientation similar to the "kidney" view sometimes seen in single particle projections (Harauz *et al.*, 1987).

The stalk is known to be flexible (Carazo *et al.*, 1988) and as such may assume several conformations. It was shown to contain the L7/L12 protein dimer (Strycharz *et al.*, 1978), which is thought to participate in GTP hydrolysis reactions during the elongation cycle of translation (Möller *et al.*, 1983). The stalk, together with other components involved in the translation, like the peptidyltransferase center, may comprise part of the "translational domain". The "exit domain", the site at which nascent polypeptides emerge out of the ribosome (Bernabeu & Lake, 1982) has been suggested to be roughly opposite to the translational domain. Because in eukaryotic ribosomes the exit domain contains a membrane attachment site (Lake *et al.*, 1974), it might be speculated that the interaction with the underlying phospholipid film occurs *via* the corresponding site in the presently studied prokaryotic ribosomes. Such interaction sites may be detected in future three-dimensional reconstructions.

There are several low density regions within the projected outline of the reconstruction. These may be interpreted as solvent regions. It has been suggested that a significant fraction of the volume of the 50 S ribosomal subunit may be empty. Part of this void volume is thought to constitute a tunnel, which provides the protected path of the nascent polypeptides (Milligan & Unwin, 1986; Yonath *et al.*, 1987). We speculate that the low density region indicated by the arrow (labeled as T in Figure 5) points roughly at the possible entrance to that tunnel. The path of the tunnel through the ribosome, however, cannot be traced from this map, due to the ambiguity inherent in a projection map alone.

Additional outstanding features are several strong scattering densities which can be well-localized. Given that a major fraction of the mass of the ribosome is rRNA, one may hypothesize that these high scattering density regions are partially accounted for by rRNA. Kühlbrandt & Unwin (1982) determined at very low resolution that in eukaryotic ribosomes a large fraction of the rRNA mass lies close to the interface between the large and small ribosome subunits. Frank *et al.* (1991) also observed a complex distribution of higher densities in the interior of prokaryotic ribosomes, which was assigned as rRNA. The resolution limits of both studies are too low to resolve rRNA regions which are not so dense, but may be essential for the function of the ribosome. Although our resolution is much higher, a projection map alone is insufficient to make precise assignments in the dense regions, but, compared to previous interpretations (reviewed by Yonath & Berkovitch-Yellin, 1993), there is a high probability that some of them lie within the overall region known as translational domain. This finding is in accord with the recent remarkable experiments showing that rRNA is the major component catalyzing the peptide bond formation (Noller *et al.*, 1992; Hardesty *et al.*, 1992). In addition, dense regions can be seen in the projection map in the vicinity of the internal tunnel. Evidence that nascent proteins progress through the ribosome in a RNA-rich environment has been found by biochemical studies (Gewitz *et al.*, 1988; Picking *et al.*, 1990; Hardesty *et al.*, 1992).

4. Conclusions

The studies reported here demonstrate our ability to produce two-dimensional crystalline arrays of 50 S ribosomal subunits from *B. stearothermophilus* by the monolayer technique. These results indicate clearly the viability of this approach for studying this rather complex macromolecular assembly. In general, obtaining monolayers of macromolecules involves a number of parameters which are not easily controlled, such as the chemical purity of macromolecules, lipids and solvents. In addition, serious difficulties have been encountered in transferring the fragile monolayers onto the electron microscope grids and in the production of samples with proper ice thickness. In addition to these common obstacles, the ribosomes impose specific complications, due to their instability, flexibility and their conformational and compositional heterogeneity. A major effort will be concentrated in identifying those factors which have the most critical impact on the crystallization, in order to improve the crystallinity of the arrays. Moreover we also plan to investigate modified particles, either lacking one or a few proteins, or those to which specific ligands have been bound, such as tRNA or an undecagold cluster (Weinstein *et al.*, 1989; Berkovitch-Yellin *et al.*, 1992; Hainfield, 1992); both are large enough to be visualized by electron cryomicroscopy. It may be expected that this approach, together with the recent advances in the technologies associated with imaging (i.e. the spot-scan at 400 kV electron cryomicroscope Brink *et al.*, 1992; Schmid *et al.*, 1993*b*), should indeed result in high resolution reconstructed images of ribosomal particles. Furthermore, given the phenomenon that the crystalline patches may have variable motifs due to either the chemical or crystallization conditions, it may be better to process high resolution images with the patch averaging procedure (Frank *et al.*, 1988; Morgan *et al.*, 1992; Soejima *et al.*, 1993). The electron crystallographic data, even at moderate resolution (10 Å) expected from frozen, hydrated samples, should lead to a clear separation of protein and RNA regions, as they are of different densities. These data should be most useful for initial phasing of the X-ray diffraction intensities towards the determination of the molecular structure of this important complex.

This research has been supported by NIH grants RR02250 and GM34360, the Kimmelman Center for Macromolecular Assembly at the Weizmann Institute, the William M. Keck Foundation and the Robert Welch

Foundation. A.Y. holds the Martin S. Kimmel Professorial Chair. We thank Dr Jaap Brink for his helpful comments on the manuscript.

References

Adrian, M., Dubochet, J., Lepault, J. & McDowall, A. W. (1984). Cryoelectron microscopy of viruses. *Nature (London)*, **308**, 32–36.

Arad, T., Leonard, K. R., Wittmann, H. G. & Yonath, A. (1984). Two-dimensional crystalline sheets of *B. stearothermophilus* ribosomal particles. *EMBO J.* **3**, 127–131.

Arad, T., Piefke, J., Weinstein, S., Gewitz, H. S., Yonath, A. & Wittmann, H. G. (1987). Three-dimensional image reconstruction from ordered arrays of 70 S ribosomes. *Biochimie*, **69**, 1001–1004.

Berkovitch-Yellin, Z., Wittmann, H. G. & Yonath, A. (1990). Low-resolution models for ribosomal particles reconstructed from electron micrographs of tilted two-dimensional sheets. *Acta Crystallogr. sect. B*, **46**, 637–643.

Berkovitch-Yellin, Z., Bennett, W. S. & Yonath, A. (1992). Aspects in structural studies on ribosomes. *CRC Rev. Biochem. Mol. Biol.* **27**, 403–444.

Bernabeu, C. & Lake, J. A. (1982). Nascent polypeptide chains emerge from the exit domain of the large ribosomal subunit; immune mapping of the nascent chain. *Proc. Nat. Acad. Sci., U.S.A.* **79**, 3111–3115.

Brink, J., Chiu, W. & Doughtery, M. (1992). Computer-controlled spot-scan imaging of crotoxin complex crystals with 400 keV electrons at near-atomic resolution. *Ultramicroscopy*, **46**, 229–240.

Capel, M. S., Kjelggaard, M., Englman, D. M. & Moore, P. B. (1988). Positions of S2, S13, S16, S17, S19 and S21 in the 30 S ribosomal subunit from *Escherichia coli*. *J. Mol. Biol.* **200**, 65–87.

Carazo, J. M., Wagenknecht, T., Radermacher, M., Mandiyan, V., Boublik, M. & Frank, J. (1988). Three-dimensional structure of 50 S *E. coli* subunit depleted of protein L7/L12. *J. Mol. Biol.* **201**, 393–404.

Chiu, W. (1986). Electron microscopy of frozen hydrated biological specimens. *Annu. Rev. Biophys.* **15**, 237–257.

Chiu, W. (1993). What does electron cryomicroscopy provide that X-ray crystallography and NMR spectroscopy cannot? *Annu. Rev. Biophys. Biomol. Struct.* **22**, 233–255.

Clark, W., Leonard K. & Lake, J. (1982). Ribosomal crystalline arrays of large subunits from *E. coli*. *Science*, **216**, 999–1000.

Darst, S. A., Ahlers, M., Meller, P. H., Kubalek, E. W., Blankenburg, R., Ribi, H. O., Ringsdorf, H. & Kornberg, R. D. (1991*a*). Two-dimensional crystals of streptavidin on biotinylated lipid layers and their interactions with biotinylated macromolecules. *Biophys. J.* **59**, 387–396.

Darst, S. A., Edwards, A. M., Kubalek, E. W. & Kornberg, R. D. (1991*b*). Three-dimensional structure of yeast RNA polymerase II at 16 Å resolution. *Cell*, **66**, 121–128.

Dubochet, J., Adrian, M., Chang, J.-J., Homo, J.-C., Lepault, J., McDowall, A. W. & Schultz, P. (1988). Cryo-electron microscopy of vitrified specimens. *Quart. Rev. Biophys.* **21**, 129–228.

Frank, J., Chiu, W. & Degn, L. (1988). The characterization of structural variations within a crystal field. *Ultramicroscopy*, **26**, 345–360.

Frank, J., Verschoor, A., Radermacher, M. & Wagenknecht, T. (1990). Morphologies of eubacterial and eucaryotic ribosomes as determined by three-dimensional electron microscopy. In *The Ribosome: Structure, Function and Evolution* (Hill, W. E., Dahlberg, A., Garrett, R. A., Moore, P. B., Schlessinger, D. & Warner, J. R., eds), pp. 107–113, Amer. Soc. for Microbiol., Washington, D.C.

Frank, J., Penczek, P., Grassucci, R. & Srivastava, S. (1991). Three-dimensional reconstruction of the 70 S *Escherichia coli* ribosome in ice: the distribution of ribosomal RNA. *J. Cell Biol.* **115**, 597–605.

Gewitz, H. S., Glotz, C., Piefke, J. Yonath, A. & Wittmann, H. G. (1988). Two-dimensional crystalline sheets of *Bacillus stearothermophilus* 50 S ribosomal subunits containing a nascent polypeptide chain. *Biochimie*, **70**, 645–648.

Hainfield, J. F. (1992). Site-specific cluster labels. *Ultramicroscopy*, **46**, 135–144.

Harauz, G., Stoeffler-Meilicke, M. & van Heel, M. (1987). Characteristic views of prokaryotic 50 S ribosomal subunits. *J. Mol. Evol.* **26**, 347–357.

Hardesty, B. & Kramer, G. (1986). Editors of *Structure, Function and Genetics of Ribosomes*. Springer Verlag, Heidelberg.

Hardesty, B., Odom, O. W. & Picking, W. (1992). Ribosome function determined by fluorescence. *Biochimie*, **74**, 391–401.

Henderson, R. (1992). Image contrast in high-resolution electron microscopy of biological macromolecules: TMV in ice. *Ultramicroscopy*, **46**, 1–18.

Henderson, R., Baldwin, J. M., Downing, K. H., Lepault, J. & Zemlin, F. (1986). Structure of purple membrane from *Halobacterium halobium*: recording, measurement and evaluation of electron micrographs at 3·5 Å resolution. *Ultramicroscopy*, **19**, 147–178.

Henderson, R., Baldwin, J. M., Ceska, T. A., Zemlin, F., Beckmann, E. & Downing, K. H. (1990). Model for the structure of bacteriorhodopsin based on high-resolution electron cryo-microscopy. *J. Mol. Biol.* **213**, 899–929.

Hill, E. W., Dahlberg, A., Garrett, R. A., Moore, P. B., Schlessinger, D. & Warner, J. R. (1990). Editors of *The Ribosome: Structure, Function and Evolution*. Amer. Soc. for Microbiol., Washington, D.C.

Jap, B. K., Zulauf, M., Scheybani, T., Hefti, A., Baumeister, W., Aebi, U. & Engel, A. (1992). 2-D crystallization: from art to science. *Ultramicroscopy*, **46**, 45–84.

Jeng, T. W. & Chiu, W. (1983). Low dose electron microscopy of the crotoxin complex thin crystal. *J. Mol. Biol.* **164**, 329–346.

Jeng, T. W., Talmon, Y. & Chiu, W. (1988). Containment system for the preparation of vitrified-hydrated virus specimens. *J. Electron Microsc. Tech.* **8**, 343–348.

Kornberg, R. D. & Darst, S. A. (1991). Two-dimensional crystals of proteins on lipid layers. *Curr. Opin. Struct. Biol.* **1**, 632–646.

Kubalek, E. W., Kornberg, R. D. & Darst, S. A. (1991). Improved transfer of two-dimensional crystals from the air/water interface to specimen support grids for high-resolution analysis by electron microscopy. *Ultramicroscopy*, **35**, 295–304.

Kuhlbrandt, W. & Unwin, P. N. T. (1982). Distribution of RNA and proteins in crystalline eucaryotic ribosomes. *J. Mol. Biol.* **156**, 611–617.

Lake, J. A., Nonomura, Y. & Sabatini, D. D. (1974). Ribosome structure as studied by electron microscopy. In *Ribosomes* (Nomura, M., Tissieres, A. &

Lengyel, P., eds), pp. 543–557, Cold Spring Harbor Laboratory Press, Cold Spring Harbor, NY.

May, R. P., Novotny, V., Novotny, P., Voss, H. & Nierhaus, K. (1992). Inter-protein distances within the large ribosomal subunit from *E. coli* ribosomes. *EMBO J.* **11**, 373–378.

Milligan, R. A. & Unwin, P. N. T. (1986). Location of exit channel for nascent protein in 80 S ribosome. *Nature (London)*, **319**, 693–695.

Möller, W., Schrier, P. I., Maasen, J. A., Zantema, A., Schop, E., Reinalda, H., Cremers, A. F. M. & Mellema, J. E. (1983). Ribosomal proteins L7/L12 of *Escherichia coli*: localization and possible molecular mechanism in translation. *J. Mol. Biol.* **163**, 553–573.

Morgan, D. G., Grant, R. A., Chiu, W. & Frank, J. (1992). Patch averaging of electron images of gp32*I crystals with variable thickness. *J. Struct. Biol.* **108**, 245–256.

Noller, H. F., Hoffarth, V. & Zimniak, L. (1992). Unusual resistance of peptidyl transferase to protein extraction procedures. *Science*, **256**, 1416–1419.

Picking, W. D., Odom, O. W. & Hardesty, B. (1992). Evidence for RNA in the peptidyl transferase center of *Escherichia coli* ribosomes as indicated by fluorescence. *Biochemistry*, **31**, 12565–12570.

Radermacher, M., Srivastava, S. & Frank. J. (1992). The structure of the 50 S ribosomal subunit from *E. coli* in frozen hydrated preparation reconstructed with secret. *Electron Microscopy*, vol. 3, pp. 19–20, EUREM 92, Granada, Spain.

Robinson, J. P., Schmid, M. F., Morgan, D. G. & Chiu, W. (1988). Three dimensional structural analysis of tetanus toxin by electron crystallography. *J. Mol. Biol.* **200**, 367–375.

Schmid, M. F., Matsudaira, P., Jeng, T. W., Jakana, J., Towns-Andrews, E., Bordas, J. & Chiu, W. (1991). Crystallographic analysis of acrosomal bundle from Limulus sperm. *J. Mol. Biol.* **221**, 711–725.

Schmid, M. F., Dargahi, R. & Tam, M. W. (1993*a*). SPECTRA: a system for processing electron images of crystals. *Ultramicroscopy*, **48**, 251–264.

Schmid, M. F., Jakana, J., Matsudaira, P. & Chiu, W. (1993*b*). Imaging frozen, hydrated acrosomal bundle from Limulus sperm at 7 Å resolution with a 400 kV electron cryomicroscope. *J. Mol. Biol.* **230**, 384–386.

Schmid, M. F., Robinson, J. P. & DasGupta, B. R. (1993*c*). Direct visualization of botulinum toxin-induced channels in phospholipid vesicles. *Nature (London)*, **364**, 827–830.

Soejima, T., Sherman, M. B., Schmid, M. F. & Chiu, W. (1993). 4 Å projection map of bacteriophage T4 DNA helix-destabilizing protein (gp32*I) crystal by 400-kV electron cryomicroscopy. *J. Struct. Biol.* **111**, 9–16.

Strycharz, W. A., Nomura, M. & Lake, J. A. (1978). Ribosomal proteins L7/L12 localized at a single region of the large subunit by immune electron microscopy. *J. Mol. Biol.* **126**, 123–140.

Taylor, K. A. & Taylor, D. W. (1993). Projection image of smooth muscle α-actinin from two-dimensional crystals formed on positively charged lipid layers. *J. Mol. Biol.* **230**, 196–205.

Tumminia, S. J., Mandiyan, V., Wall, J. S. & Boublik, M. (1991). Heterogeneity of *Escherichia coli* ribosomes established by scanning transmission electron microscopy. *Biochemie*, **73**, 919–925.

Verschoor, A., Frank, J. & Boublik, M. (1985). Investigation of the 50 S ribosomal subunit by electron microscopy and image analysis. *J. Ultrastruct. Res.* **92**, 180–189.

von Böhlen, K., Makowski, I., Hansen, H. A. S., Bartels, H., Berkovitch-Yellin, Z., Zaytzev-Bashan, A., Meyer, S., Paulke, C., Franceschi, F. & Yonath, A. (1991). Characterization and preliminary attempts for derivatization of crystals of large ribosomal subunits from *H. marismortui* diffracting to 3 Å resolution. *J. Mol. Biol.* **222**, 11–15.

Weinstein, S., Jahn, W., Wittmann, H. G. & Yonath, A. (1989). Novel procedures of derivatization of ribosomes for crystallographic studies. *J. Biol. Chem.* **264**, 19138–19142.

Yonath, A. & Berkovitch-Yellin, Z. (1993). Hollows, voids, gaps and tunnels in the ribosome. *Curr. Opin. Struct. Biol.* **3**, 175–181.

Yonath, A. & Wittmann, H. G. (1989). Challenging the three-dimensional structure of ribosomes. *Trends Biochem. Sci.* **14**, 329–335.

Yonath, A., Leonard, K. R. & Wittmann, H. G. (1987). A tunnel in the large ribosomal subunit revealed by three-dimensional image reconstruction. *Science*, **236**, 813–816.

Zhou, Z. H. (1993). Determination of the defocus value of micrographs of ice-embedded specimen without carbon support film. In *51st Annual Meeting of the Microscopical Society of America*, pp. 560–561, Cincinatti, San Francisco Press, Inc., CA.

Edited by M. F. Moody

(Received 7 October 1993; accepted 5 April 1994)